

# MAPL: Memory Augmentation and Pseudo-Labeling for Semi-Supervised Anomaly Detection

1<sup>st</sup> Junzhuo Chen  
*School of Artificial Intelligence*  
*Hebei University of Technology*  
Tianjin, China  
jzchen7@foxmail.com

2<sup>nd</sup> Zhixin Lu  
*College of Big Data*  
*Weifang Institute of Technology*  
Weifang, China  
11179484365@163.com

3<sup>rd</sup> Shitong Kan  
*School of Artificial Intelligence*  
*Hebei University of Technology*  
Tianjin, China  
2601549919@qq.com

**Abstract**—A new methodology, Memory Augmentation and Pseudo-Labeling (MAPL), is introduced to tackle the challenges of large unlabeled data and difficult-to-identify anomalies in industrial settings. An anomaly simulation strategy is introduced to enhance the model's ability to detect rare or unknown anomaly types by generating simulated samples. To address the lack of labeled anomalous samples, a pseudo-labeler method based on a one-classifier ensemble was employed, improving model robustness with limited data by selecting key pseudo-labeling hyperparameters. A memory-enhanced learning mechanism is also integrated to predict abnormal regions by comparing input samples with normal samples stored in a memory pool. An end-to-end learning framework is employed by MAPL to directly identify abnormal regions from input data, optimizing detection efficiency and real-time performance. Extensive trials on the BHAD dataset show that MAPL achieves an average image-level AUROC score of 86.2%, a 5.1% improvement over the original MemSeg [4] model.

**Source code:** <https://github.com/jzc777/MAPL>.

**Keywords**—Anomaly Detection, Computer Vision, Semi supervised algorithm, Deep learning

## I. INTRODUCTION

Efficient product surface defect detection is essential for maintaining quality and efficiency in today's industrial production. With the rapid advancement of automation, traditional inspection methods are inadequate, necessitating automatic detection technologies. Deep learning has significantly improved defect identification, yet challenges remain in detecting minor defects in industrial images due to their unique distribution characteristics.

Accurately identifying minor defects is a major challenge in industrial anomaly detection. Traditional techniques often rely on distance measurements, such as reconstruction error analysis of autoencoders, assuming that anomalies significantly differ from normal data during reconstruction. Methods include structural similarity indices, dual autoencoders in GANs, multi-head variational autoencoders with discriminators, and autoencoders for nonlinear dimensionality reduction. GANs are popular in unsupervised anomaly detection, with advancements in adversarial autoencoders and encoder optimization enhancing efficiency. While deep learning and nearest-neighbor methods have enhanced detection performance in natural image models [5], identifying tiny defects in industrial images remains challenging due to differences in image distribution. Sub-image anomaly detection based on depth pyramid correspondence has significantly improved positioning accuracy in industrial applications [6]. Additionally, embedding-based approaches [5-8] and knowledge distillation techniques [9-14] can extract valuable knowledge from

sophisticated pre-trained models, but they face challenges in effectively transferring this knowledge to specific industrial applications, hindering the adaptability and efficiency of the models in practical environments.

Existing semi-supervised and GAN-based methods, though improving anomaly detection accuracy, heavily rely on extensive labeled datasets and clear anomaly feature distinctions. These methods struggle with subtle anomalies or limited labeled data, and current techniques have notable limitations in model adaptability and data utilization.

To address these challenges, particularly large-scale unlabeled data and subtle anomalies in industrial scenarios, this paper proposes MAPL. MAPL combines a highly efficient semi-supervised learning framework with advanced pseudo-labeling method, which significantly improves the model's generalization ability and learning efficiency in complex industrial environments. The method utilizes an adapted VAE/GAN [15] encoder and memory augmentation network to directly identify anomalous regions in the input image by simulating anomalous samples, which optimizes the inference process and meets the real-time requirements. Moreover, by incorporating SPADE's [16] pseudo-labeling method, MAPL not only simplifies the training process but also employs consistency checks to optimize pseudo-labeling, effectively utilizing simulated anomalous samples to boost data efficiency and model generalization.

To evaluate MAPL's efficiency, a new dataset, BHAD, was created for industrial surface defect detection. It samples from existing datasets like MVTec AD, Visa, and MDPP, adding random white noise to simulate various production interference scenarios. This approach enhances the complexity of the inspection task and the practical relevance of the study's findings.

In summary, the main contributions of this paper include the following four aspects:

- Proposed MAPL, a combination of semi-supervised learning method and pseudo-labeling method, effectively improves the model's ability to process unlabeled large-scale data and identify minor anomalies.
- The encoder structure based on VAE/GAN is adopted and the LeakyReLU activation function is uniformly used to optimize the accuracy of industrial defect detection.
- The anomaly simulation strategy is adopted to generate abnormal samples, which are used to train the anomaly detection module and pseudo-labeler, improving the generalization ability of the model.

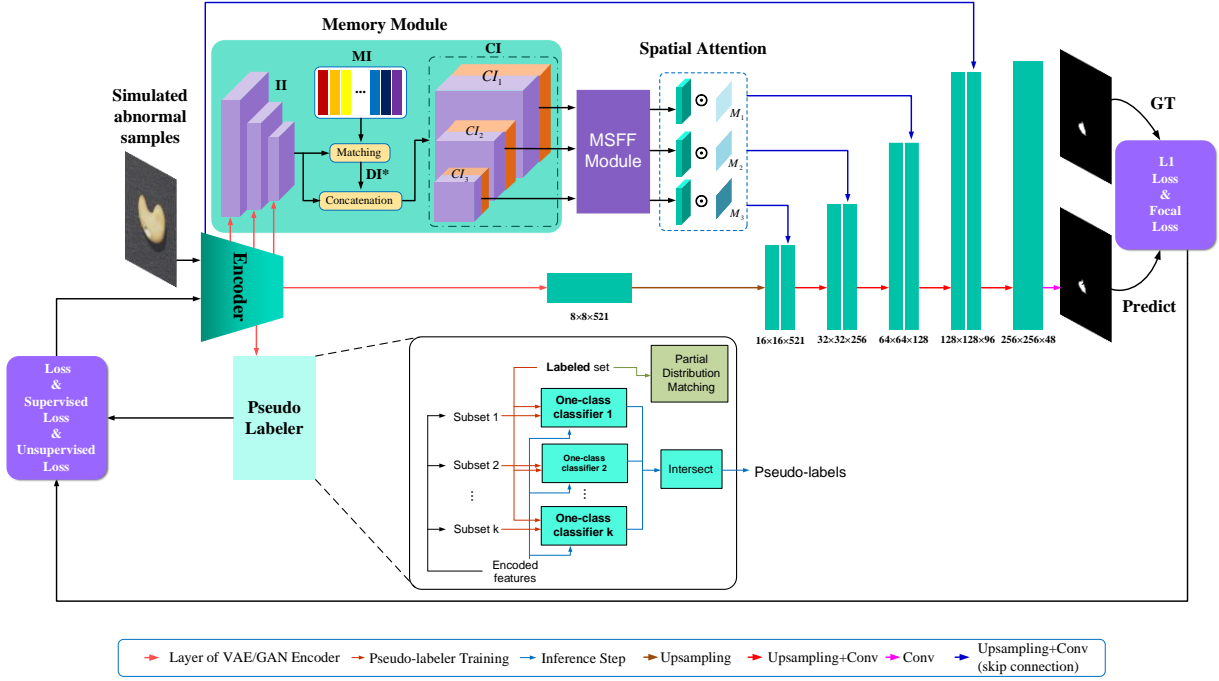


Fig. 1. Overview of the MAPL model, which is based on the Memseg framework and incorporates an adapted VAE/GAN encoder and LeakyReLU activation function, and introduces a pseudo labeler to enhance robustness, improving the adaptability to anomaly simulation datasets and anomaly detection efficacy.

- Experiments on the newly constructed BHAD data set verified the high accuracy and robustness of the MAPL method in industrial defect detection.

In the subsequent sections, the general framework and key components of the methodology will be described in Section II. In Section III, comparative and ablation experiments will be performed and the results will be analyzed. Finally, in Section IV, the conclusions of the study will be presented.

## II. METHODOLOGY

This section introduces the MAPL model (Fig.1) using an encoder-decoder structure for semantic segmentation and anomaly detection, using a modified VAE/GAN-based architecture with LeakyReLU [17]. During training, MAPL simulates anomalies by altering normal samples  $I$ , creating an anomalous dataset  $\mathcal{D}^a$  for training. The encoder  $h$  converts input features  $\mathbf{x}$  into latent representations  $\mathbf{r} = h(\mathbf{x})$ , from which the predictor computes the anomaly score  $q(\mathbf{r})$ .

Pseudo-labelers  $v$  assign labels to the simulated anomalies, optimizing data  $\mathbf{x}^a$  utilization through binary cross-entropy losses  $L_{y^a}$ ,  $L_{y^l}$  for both labeled and pseudo-labeled data. The memory bank  $\mathbf{MB}$  stores features from normal samples, and during inference, computes the L2 distance between new input features  $\mathbf{x}$  and stored memory information  $\mathbf{MI}$  to identify potential anomalies. This connection information  $\mathbf{CI}$  is processed by the Multi-scale Feature Fusion (MSFF) module, where  $3 \times 3$  convolutional layers adjust feature map resolutions for fusion.

The spatial attention maps utilize the minimum difference value  $\mathbf{DI}^*$  to generate three spatial attention maps, denoted as  $M_n$ , which weight the MSFF-processed information  $\mathbf{CI}$  before it is passed to the decoder. The loss function module employs a composite approach, integrating L1 loss  $L_{l1}$ , focus

loss  $L_f$ , and pseudo labeler-specific binary cross-entropy losses  $L_{y^a}$  and  $L_{y^l}$ , collectively optimizing the model's performance.

### A. Abnormal Simulation

The MAPL MemSeg uses a self-supervised approach to simulate anomaly patterns in industrial scenes through three key steps. First, a binary mask  $M_1$  is generated from the input image  $I$  using threshold binarization combined with Perlin noise. Then, the background is formed and combined with a noisy foreground  $I'_n$ , which integrates texture from the DTD dataset[18] and structural alterations. This process ensures that the simulated anomalies  $I_A$  closely resemble real-world conditions, thereby enhancing MAPL's ability to detect actual anomalies.

### B. Pseudo Labeler

#### 1) Pseudo Labeler Architecture and Training

The pseudo-labeler includes models  $\text{OCCs}(o_1, o_2, \dots, o_K)$ , each trained with negative data ( $\mathcal{D}_0^l$ ), and one of  $K$  anomalous simulation subsets ( $\mathcal{D}_1^a, \mathcal{D}_2^a, \dots, \mathcal{D}_K^a$ ). The anomaly score  $o_k(\mathbf{x})$  is generated. If all OCCs agree, positive pseudo-labels are assigned to  $v(h(\mathbf{x}^a)) = 1$ , if  $\prod_{k=1}^K \hat{y}_k^{pa} = 1$ , where

$$\hat{y}_k^{pa} = 1 \quad \text{if } o_k(h(\mathbf{x}^a)) > \eta_k^p \quad (1)$$

and negative pseudo-labels are assigned if  $\prod_{k=1}^K \hat{y}_k^{na} = 1$ ,

then  $v(h(\mathbf{x}^a)) = 0$ , where

$$\hat{y}_k^{na} = 1 \quad \text{if } o_k(h(\mathbf{x}^a)) < \eta_k^p \quad (2)$$

data without consensus is labeled as unknown.

## 2) Regarding the selection of thresholds $\eta^p$ and $\eta^n$

SPADE estimates the marginal distribution of anomalies using a partial matching method. Thresholds  $\eta^p$  and  $\eta^n$  are determined by minimizing the Wasserstein distance  $D_w$  between the abnormal score distributions of simulated and labeled data

$$\eta_k^p = \arg \min_{\eta} D_w(\{o_k(h(\mathbf{x}^l) | y^l = 1), \{o_k(h(\mathbf{x}^a) > \eta)\}) \quad (3)$$

$$\eta_k^n = \arg \min_{\eta} D_w(\{o_k(h(\mathbf{x}^l) | y^l = 0), \{o_k(h(\mathbf{x}^a) < \eta)\}) \quad (4)$$

## C. Memory Module

The MAPL model's memory module mimics the human process of anomaly detection by comparing observed images with stored normal images. Normal images are used as memory samples to extract features at resolutions  $N \times 64 \times 64$ ,  $N \times 128 \times 32 \times 32$ , and  $N \times 256 \times 16 \times 16$ , forming the  $MI$ . During training or inference, the input image features  $\mathbf{x}$  are also extracted at these resolutions.

The L2 distance between the input image and memory samples is calculated to derive the difference information  $DI$  as follows:

$$DI = \bigcup_{i=1}^N \|MI_i - \mathbf{x}\|_2 \quad (5)$$

Where  $N$  is the number of memory samples. The minimum L2 distance identifies potential anomalies, and the optimal difference information  $DI^*$  is given by:

$$DI^* = \underset{DI_i \in DI}{\operatorname{argmin}} \sum_{x \in DI_i} x \quad (6)$$

Higher  $DI^*$  values suggest a greater likelihood of anomalies. Features  $DI^*$  and  $\mathbf{x}$  are concatenated, processed by the MSFF module, and then passed to the decoder  $g$  via U-Net's skip connections for final anomaly detection.

## D. Spatial Attention Map

The method constructs three spatial attention maps  $M_1$ ,  $M_2$  and  $M_3$  to enhance the detection of anomalies by utilizing disparity information. These maps are derived from feature maps of varying sizes:  $(16 \times 16, 32 \times 32, \text{ and } 64 \times 64)$ .

- $M_3$  is obtained from the  $16 \times 16$  feature map.
- $M_2$  is produced by up-sampling  $M_3$  and element-wise multiplication with the  $32 \times 32$  feature map.
- $M_1$  derived from  $M_2$  through up-sampling and multiplication with the  $64 \times 64$  feature map.

Each spatial attention map is then individually weighted via MSFF to generate the corresponding information  $CI$ .

## E. Multi-Scale Feature Fusion Module

The model employs a combination of channel attention and multi-scale feature fusion [19] to enhance visual and semantic information in  $CI$ . The fusion process begins with a  $3 \times 3$  convolutional layer to maintain channel consistency. Despite initial expectations, Coordinate Attention (CA)[20]

was found to be ineffective in improving performance and was therefore removed to reduce computational load.

Feature maps of different dimensions are aligned through up-sampling and convolution, followed by MSFF via element-wise summation. Finally, the fused features are multiplied by the spatial attention map  $M_n$  and fed into the decoder, improving the model's ability to handle complex scenarios.

## F. Loss Function and Optimization

### 1) Composite Loss Function Design and Application

The MAPL model employs a combination of L1 loss and focal loss to maintain pixel uniformity and improve segmentation, especially in challenging areas. L1 loss preserves edge details, while focal loss adjusts the weights between normal and abnormal regions. The composite objective function  $L_m$  combines these loss functions, defined as:

$$L_m = \omega_{l1} L_{l1} + \omega_f L_f \quad (7)$$

where  $\omega_{l1}$  and  $\omega_f$  are weighting factors. The composite function merges L1 and focal loss and incorporates the pseudo labeler's loss to improve handling of simulated anomalies.

### 2) Pseudo Labeler Loss Function Strategy

In pseudo-label training, both supervised and unsupervised Binary Cross-Entropy (BCE) loss functions are used to improve the model's performance. The supervised loss function is applied to labeled data, while the unsupervised loss function is used for pseudo-labeled data.

The final training objective combines these losses with the MAPL loss to optimize the model:

$$L_{all} = L_m + L_{y^u} + L_{y^l} \quad (8)$$

where  $L_m$  is the MemSeg loss,  $L_{y^u}$  is the supervised BCE loss, and  $L_{y^l}$  the unsupervised BCE loss.

### 3) Training optimization and convergence monitoring

During model training, the combined loss function  $L_{all}$  is applied, designed to optimize encoder ( $h$ ), predictor ( $q$ ), Memory bank ( $MB$ ), MSFF ( $MF$ ) and Decoder ( $g$ ).

$$h^*, q^*, MB^*, MF^*, g^* = \arg \min_{h,q,MB,MF,d} L_{all} \quad (9)$$

Throughout training, loss fluctuations are closely monitored. If the loss does not significantly decline over several iterations, it may indicate that the model is nearing convergence. At this point, training can be stopped, or parameters like the learning rate can be adjusted to further improve model performance.

## III. EXPERIMENT

### A. Dataset

To accurately assess the effectiveness and feasibility of the proposed MAPL method, this study developed a new dataset called BHAD (Benchmark for High precision Anomaly Detection)[21]. BHAD is designed to provide a comprehensive evaluation of the MAPL Net approach, integrating elements from established datasets like MVTEC

AD [1], Visa[2], and MDPP[3]. It includes four object types, with 369 to 432 normal training samples and test images containing both normal and abnormal samples. The test set features authentic faults with varied textures and sizes to thoroughly evaluate detection capabilities.

A specialized exception mask configuration is applied, considering factors like mask usage, background threshold adjustment, and inversion, to enhance data preprocessing. To simulate real-world industrial scenarios, random Gaussian noise and contrast modifications were introduced to the images, improving the model’s ability to handle environmental interference. Performance is evaluated using image-level AUC-ROC metrics to ensure precision and reliability.

### B. Experimental Environment and Hyperparameter Settings

The experimental environment configuration is shown in Table 1:

Name	Parameter
CPU	Xeon(R) Gold 6430 CPU
RAM	120 GB
GPU	NVIDIA RTX 4090 (24 GB)
CUDA	12.1
Deep learning framework	PyTorch 2.1.0

Table 1: Detailed configuration parameters of experimental environment

The following strategies, as shown in Table 2, are adopted to ensure the efficient training of the MAPL model:

Hyper-parameters	Parameter
Iteration steps	500
Batch_size	8 (4 normal, 4 simulated abnormal)
Image_size	256×256
Learning rate	0.003
L1 Loss weighting	0.6
Focus Loss weighting	0.4
Memory samples	30
OCC settings	Gaussian Mixture Model (GMM)
Number of OCC	2

Table 2: Parameter configuration for model training

The learning rate is initially set to 0.003 through grid search, followed by a warm-up adjustment and dynamic decay using the cosine annealing algorithm. To balance the model’s capability in handling different anomaly types, texture and structure anomaly simulations are performed with equal probability. The number of training rounds for the pseudo labeler is dynamically adjusted based on dataset size to ensure effective GMM updates during each data iteration.

### C. Comparative Experiment

On the BHAD dataset, MAPL outperforms the original MemSeg model in terms of image-level ROC-AUC scores. As shown in Table 3, MAPL achieves higher performance in all subcategories, especially in the Cashew and Leather categories.

Datasets	Bracket black	Cashew	Leather	Screw	Average
Memseg	75.23	78.00	96.71	74.46	81.10
MAPL (Ours)	<b>81.07</b>	<b>87.17</b>	<b>98.78</b>	<b>76.67</b>	<b>86.20</b>

Table 3: Image-level ROC-AUC % performance comparison between MAPL and MemSeg on the BHAD

### D. Ablation Experiments

Ablation experiments play an imperative role in evaluating the impact of various model components on overall performance. This study specifically focuses on whether or not to remove the effects of CA, spatial attention maps, and MSFF. The following are the primary experiments conducted:

Datasets	Bracket black	Cashew	Leather	Screw	Average
No msff	75.23	78.00	96.71	74.46	82.28
Added CA	<b>81.07</b>	<b>87.17</b>	98.78	76.67	85.92
No Spatial Attention	46.04	78.89	<b>99.35</b>	71.12	73.85
MAPL (Ours)	78.01	85.62	99.21	<b>81.96</b>	<b>86.2</b>

Table 4: Image-level ROC-AUC % performance comparison of MAPL’s ablation experiments on the BHAD .

## IV. CONCLUSION

The paper proposes the MAPL model, which obtains an average image-level AUROC score of 86.2% on the BHAD dataset. This model significantly improves the accuracy and resilience of industrial surface defect identification, particularly in challenging conditions with noise interference. Ablation experiments were conducted to evaluate the impact of key components—MSFF, CA, and spatial attention maps—on model performance. The results demonstrate that removing MSFF significantly decreases the average AUROC to 82.28%, underscoring its importance for feature fusion and reducing information redundancy. Although CA slightly improves performance, its exclusion results in the highest average AUROC, suggesting that the MAPL model performs better without it. The removal of spatial attention maps led to a notable decline in performance, highlighting their critical role in identifying abnormal regions. Based on these findings, the MAPL model was optimized by excluding CA while retaining MSFF and spatial attention maps. This configuration enhances computational efficiency and maintains high performance, achieving an average AUROC of 86.2% across all test conditions, thereby confirming the synergistic effect of the selected components.

This outcome demonstrates MAPL’s efficacy in handling noise interference and offers new methodologies for industrial anomaly detection. Further optimization and validation in real-world environments are needed. Therefore, future work will concentrate on expanding the application scenarios and improving the model by incorporating additional practical environments for further validation and optimization of the MAPL model. These explorations will tackle the current restrictions and improve the model’s capacity to generalize and be practically applied.

In summary, this research tackles the challenges of handling unlabeled large-scale data and detecting difficult-to-identify anomalies in industrial settings.

## REFERENCES

- [1] P. Bergmann, M. Fauser, D. Sattlegger, and C. Steger, "MVTec AD - A Comprehensive Real-World Dataset for Unsupervised Anomaly Detection," presented at the Proceedings of the IEEE/CVF Conference on Computer Vision and Pattern Recognition, 2019, pp. 9592–9600. Accessed: Feb. 15, 2024. [Online]. Available: [https://openaccess.thecvf.com/content\\_CVPR\\_2019/html/Bergmann\\_MVTec\\_AD\\_-\\_A\\_Comprehensive\\_Real-World\\_Dataset\\_for\\_Unsupervised\\_Anomaly\\_CVPR\\_2019\\_paper.html](https://openaccess.thecvf.com/content_CVPR_2019/html/Bergmann_MVTec_AD_-_A_Comprehensive_Real-World_Dataset_for_Unsupervised_Anomaly_CVPR_2019_paper.html)
- [2] Y. Zou, J. Jeong, L. Pemula, D. Zhang, and O. Dabeer, "SPot-the-Difference Self-supervised Pre-training for Anomaly Detection and Segmentation," in *Computer Vision – ECCV 2022*, Springer, Cham, 2022, pp. 392–408. doi: 10.1007/978-3-031-20056-4\_23.
- [3] S. Jezek, M. Jonak, R. Burget, P. Dvorak, and M. Skotak, "Deep learning-based defect detection of metal parts: evaluating current methods in complex conditions," in *2021 13th International Congress on Ultra Modern Telecommunications and Control Systems and Workshops (ICUMT)*, Oct. 2021, pp. 66–71. doi: 10.1109/ICUMT54235.2021.9631567.
- [4] M. Yang, P. Wu, and H. Feng, "MemSeg: A semi-supervised method for image surface defect detection using differences and commonalities," *Eng. Appl. Artif. Intell.*, vol. 119, p. 105835, Mar. 2023, doi: 10.1016/j.engappai.2023.105835.
- [5] L. Bergman, N. Cohen, and Y. Hoshen, "Deep Nearest Neighbor Anomaly Detection," arXiv.org. Accessed: Mar. 20, 2024. [Online]. Available: <https://arxiv.dosf.top/abs/2002.10445v1>
- [6] N. Cohen and Y. Hoshen, "Sub-Image Anomaly Detection with Deep Pyramid Correspondences," arXiv.org. Accessed: Mar. 20, 2024. [Online]. Available: <https://arxiv.dosf.top/abs/2005.02357v3>
- [7] Y. Zheng, X. Wang, R. Deng, T. Bao, R. Zhao, and L. Wu, "Focus Your Distribution: Coarse-to-Fine Non-Contrastive Learning for Anomaly Detection and Localization," in *2022 IEEE International Conference on Multimedia and Expo (ICME)*, Jul. 2022, pp. 1–6. doi: 10.1109/ICME52920.2022.9859925.
- [8] K. Roth, L. Pemula, J. Zepeda, B. Schölkopf, T. Brox, and P. Gehler, "Towards Total Recall in Industrial Anomaly Detection," presented at the Proceedings of the IEEE/CVF Conference on Computer Vision and Pattern Recognition, 2022, pp. 14318–14328. Accessed: Mar. 21, 2024. [Online]. Available: [https://openaccess.thecvf.com/content/CVPR2022/html/Roth\\_Towards\\_Total\\_Recall\\_in\\_Industrial\\_Anomaly\\_Detection\\_CVPR\\_2022\\_paper.html](https://openaccess.thecvf.com/content/CVPR2022/html/Roth_Towards_Total_Recall_in_Industrial_Anomaly_Detection_CVPR_2022_paper.html)
- [9] T. Defard, A. Setkov, A. Loesch, and R. Audigier, "PaDiM: A Patch Distribution Modeling Framework for Anomaly Detection and Localization," in *Pattern Recognition. ICPR International Workshops and Challenges*, Springer, Cham, 2021, pp. 475–489. doi: 10.1007/978-3-030-68799-1\_35.
- [10] M. Salehi, N. Sadjadi, S. Baselizadeh, M. H. Rohban, and H. R. Rabiee, "Multiresolution Knowledge Distillation for Anomaly Detection," presented at the Proceedings of the IEEE/CVF Conference on Computer Vision and Pattern Recognition, 2021, pp. 14902–14912. Accessed: Mar. 21, 2024. [Online]. Available: [https://openaccess.thecvf.com/content/CVPR2021/html/Salehi\\_Multiresolution\\_Knowledge\\_Distillation\\_for\\_Anomaly\\_Detection\\_CVPR\\_2021\\_paper.html](https://openaccess.thecvf.com/content/CVPR2021/html/Salehi_Multiresolution_Knowledge_Distillation_for_Anomaly_Detection_CVPR_2021_paper.html)
- [11] G. Wang, S. Han, E. Ding, and D. Huang, "Student-Teacher Feature Pyramid Matching for Anomaly Detection," arXiv.org. Accessed: Mar. 21, 2024. [Online]. Available: <https://arxiv.dosf.top/abs/2103.04257v3>
- [12] T. D. Tien *et al.*, "Revisiting Reverse Distillation for Anomaly Detection," presented at the Proceedings of the IEEE/CVF Conference on Computer Vision and Pattern Recognition, 2023, pp. 24511–24520. Accessed: Mar. 21, 2024. [Online]. Available: [https://openaccess.thecvf.com/content/CVPR2023/html/Tien\\_Revisiting\\_Reverse\\_Distillation\\_for\\_Anomaly\\_Detection\\_CVPR\\_2023\\_paper.html](https://openaccess.thecvf.com/content/CVPR2023/html/Tien_Revisiting_Reverse_Distillation_for_Anomaly_Detection_CVPR_2023_paper.html)
- [13] H. Deng and X. Li, "Anomaly Detection via Reverse Distillation From One-Class Embedding," presented at the Proceedings of the IEEE/CVF Conference on Computer Vision and Pattern Recognition, 2022, pp. 9737–9746. Accessed: Mar. 21, 2024. [Online]. Available: [https://openaccess.thecvf.com/content/CVPR2022/html/Deng\\_Anomaly\\_Detection\\_via\\_Reverse\\_Distillation\\_From\\_One-Class\\_Embedding\\_CVPR\\_2022\\_paper.html](https://openaccess.thecvf.com/content/CVPR2022/html/Deng_Anomaly_Detection_via_Reverse_Distillation_From_One-Class_Embedding_CVPR_2022_paper.html)
- [14] T. Cao, J. Zhu, and G. Pang, "Anomaly Detection Under Distribution Shift," presented at the Proceedings of the IEEE/CVF International Conference on Computer Vision, 2023, pp. 6511–6523. Accessed: Mar. 21, 2024. [Online]. Available: [https://openaccess.thecvf.com/content/ICCV2023/html/Cao\\_Anomaly\\_Detection\\_Under\\_Distribution\\_Shift\\_ICCV\\_2023\\_paper.html](https://openaccess.thecvf.com/content/ICCV2023/html/Cao_Anomaly_Detection_Under_Distribution_Shift_ICCV_2023_paper.html)
- [15] A. B. L. Larsen, S. K. Sønderby, H. Larochelle, and O. Winther, "Autoencoding beyond pixels using a learned similarity metric," in *Proceedings of The 33rd International Conference on Machine Learning*, PMLR, Jun. 2016, pp. 1558–1566. Accessed: Feb. 15, 2024. [Online]. Available: <https://proceedings.mlr.press/v48/larsen16.html>
- [16] J. Yoon, K. Sohn, C.-L. Li, S. O. Arik, and T. Pfister, "SPADE: Semi-supervised Anomaly Detection under Distribution Mismatch," Nov. 30, 2022, *arXiv*: arXiv:2212.00173. doi: 10.48550/arXiv.2212.00173.
- [17] A. L. Maas, "Rectifier Nonlinearities Improve Neural Network Acoustic Models," 2013. Accessed: Mar. 07, 2024. [Online]. Available: <https://www.semanticscholar.org/paper/Rectifier-Nonlinearities-Improve-Neural-Network-Maas/367f2c63a6f6a10b3b64b8729d601e69337ee3cc>
- [18] M. Cimpoi, S. Maji, I. Kokkinos, S. Mohamed, and A. Vedaldi, "Describing Textures in the Wild," presented at the Proceedings of the IEEE Conference on Computer Vision and Pattern Recognition, 2014, pp. 3606–3613. Accessed: Apr. 22, 2024. [Online]. Available: [https://openaccess.thecvf.com/content\\_cvpr\\_2014/html/Cimpoi\\_Describing\\_Textures\\_in\\_2014\\_CVPR\\_paper.html](https://openaccess.thecvf.com/content_cvpr_2014/html/Cimpoi_Describing_Textures_in_2014_CVPR_paper.html)
- [19] S. Chen, Z. Cheng, L. Zhang, and Y. Zheng, "SnipeDet: Attention-guided pyramidal prediction kernels for generic object detection," *Pattern Recognit. Lett.*, vol. 152, pp. 302–310, Dec. 2021, doi: 10.1016/j.patrec.2021.10.026.
- [20] Q. Hou, D. Zhou, and J. Feng, "Coordinate Attention for Efficient Mobile Network Design," presented at the Proceedings of the IEEE/CVF Conference on Computer Vision and Pattern Recognition, 2021, pp. 13713–13722. Accessed: Apr. 24, 2024. [Online]. Available: [https://openaccess.thecvf.com/content/CVPR2021/html/Hou\\_Coordinate\\_Attention\\_for\\_Efficient\\_Mobile\\_Network\\_Design\\_CVPR\\_2021\\_paper.html](https://openaccess.thecvf.com/content/CVPR2021/html/Hou_Coordinate_Attention_for_Efficient_Mobile_Network_Design_CVPR_2021_paper.html)
- [21] J. Chen, "Benchmark for High precision Anomaly Detection," vol. 1, May 2024, doi: 10.17632/957mmybjy.1.

© 2024 IEEE. Personal use of this material is permitted. Permission from IEEE must be obtained for all other uses, in any current or future media, including reprinting/republishing this material for advertising or promotional purposes, creating new collective works, for resale or redistribution to servers or lists, or reuse of any copyrighted component of this work in other works.